Auto-Regressive Model of Magnetic Signature for Non-Invasive Fault Location in Power Systems

J.A.O Neto[1], C.A.F. Sartori[1], E. Blanco[2], J. Huillery[2]

Abstract - Our aim is to evaluate the feasibility of fault location in transmission lines by analyzing the magnetic signatures resulting from non-invasive measurements. Besides traditional monitoring methods, which use sensors physically connected to the electric power system, a non-invasive method seems an interesting way to satisfy the increasingly demanding economic and technical requirements. This paper investigates a fault location methodology based on an autoregressive modeling of the magnetic signature measured around the transmission line. The efficiency of the method is analyzed based on a simulation example which takes into account 8000 different fault scenarios.

***Index Terms*—Power systems, fault location, fault detection, non-invasive diagnostic, magnetic signature, traveling waves theory.**

I. Introduction

Electric Power Systems (EPS) are subject to undesirable transients that can be caused by lightning, drive inductive loads, switching capacitors and other phenomena. The potential faults that can appear in an EPS can cause extensive financial damages to both energy suppliers as well as to consumers. These faults may occur in different components of an EPS, among which the Transmission Lines (TL) which are the focus of the present study. Their physical dimensions, functional complexity and the environment they are built in make the TL highly susceptible elements and contribute to increasing the difficulties related to their maintenance and monitoring [1]. So as to satisfy the high technical and economic requirements, the time spent by the maintenance teams to locate and to repair the fault should be as short as possible. In this context, there has been a growing interest in the development of monitoring and diagnostic methodologies.

Some works concerning fault location using invasive approaches can be found in the literature. We can highlight the impedance calculation algorithms based on the measurement of apparent TL impedance that changes during a fault [2][3][4][5]. The measurement of the TL impedance is based on the voltage and current measured in one or multiple TL terminals. Besides, other algorithms based on the traveling wave theory which analyzes the wave propagation along the TL [6][7][8][9], as well as machine-learning techniques which identify some behavioral patterns to estimate the fault location [10][11][12][13][14][15] have been proposed.

Non-invasive approaches for fault location in EPS can provide a number of advantages: (i) a highly qualified team is not necessary to install and to connect the devices to the TL; (ii) the service does not need to be interrupted; (iii) portable measurement devices are possible; and (iv) it avoids any contact with de TL. Only few non-invasive techniques to monitor faults in EPS have been reported in the literature. We can cite two works: in [16], a wavelet analysis is used to classify the faults and, in [17], a temporal analysis is proposed to locate the faults. Both techniques are based on the magnetic signature measured around the TL. Nevertheless, new developments of non-invasive techniques for monitoring energy networks are still necessary.

We here investigate a non-invasive methodology for fault location in EPS. The method relies on the Auto-Regressive (AR) modeling of the magnetic signature and involves three steps. In the first step, the parameters of the model are identified based on a no-fault magnetic signature. In the second step, the difference between the signal predicted by the model and the true measurement is monitored and allows detecting the occurrence of a fault. In the third step, the traveling waves theory is used to locate the fault along the TL.

This paper is organized as follows: the magnetic signature is presented in part II. Part III presents the simulation of the TL and the different scenarios of faults used to evaluate the fault location methodology. The AR methodology is explained in part IV and evaluated in part V. A discussion and some conclusions are given in part VI.

II. Magnetic Field Analysis

To capture the magnetic field, we used two coils in perpendicular planes; one to monitor the field in the horizontal direction H_x and one to monitor the field in the vertical direction H_y. This section describes how to calculate the magnetic field using a system of three long wires, as shown in [18].

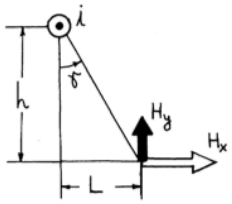

Fig. 1 - Variables for magnetic field analysis

[1] Dep. de Eng. de Energia e Automação Elétricas - Escola Politécnica da Univ. de São Paulo (PEA/EPUSP); Avenida Professor Lineu Prestes, 2468 - Butantã, São Paulo - SP, 05508-000;
Centro Tecnológico da Marinha em São Paulo (CTMSP):
e-mail: jesus.neto@usp.br / Phone :+55 11 3817-7573;
Instituto de Pesquisas Energéticas e Nucleares (IPEN/CNEN-SP):
e-mail: sartori@pea.usp.br / Phone: +55 11 3817-7391;

[2] Dép. Méthodes pour l'ingénierie des systèmes du Laboratoire Ampère (CNRS UMR 5005), Ecole Centrale de Lyon, Bât. H9, 36 Av. Guy de Collongue, 69134 Ecully ;
e-mail: eric.blanco@ec-lyon.fr / Phone : +33 4 72 18 61 01 ;
e-mail: julien.huillery@ec-lyon.fr / Phone:+33 4 72 18 61 09 ;

A long conductor carrying a current i generates a magnetic field which can be decomposed into a vertical component H_x and a horizontal component H_y, see Fig. 1. From the Ampère Circulation law, those components are defined by:

$$H_x = Di \quad and \quad H_y = Qi \qquad (1)$$

where the factors D and Q are the coefficients related to the spatial arrangement of the sensor (see [18]) given by:

$$D = \frac{(cos\,\delta)^2}{2\pi h} \quad and \quad Q = \frac{cos\,\delta\, sin\,\delta}{2\pi h} \qquad (2)$$

where:

$$\delta = tan^{-1}\frac{L}{h} \qquad (3)$$

For the three-current wires case, the horizontal H_x and vertical H_y components of the local magnetic field intensity can be determined by:

$$\begin{aligned} H_x &= D_1 i_1 + D_2 i_2 + D_3 i_3 \\ H_y &= Q_1 i_1 + Q_2 i_2 + Q_3 i_3 \end{aligned} \qquad (4)$$

Equation (4) represents the superposition of the magnetic field contributions of each conductor in the horizontal and vertical axes. The terms Q_n and D_n are the spatial arrangements of the conductor n to the sensor and i_n is the current through the conductor n. A matrix representation of that can be written as:

$$[H_{xy}] = [A_{DQ}][I_{3\phi}] \qquad (5)$$

where

$$[A_{DQ}] = \begin{bmatrix} D_1 & D_2 & D_3 \\ Q_1 & Q_2 & Q_3 \end{bmatrix} \qquad (6)$$

and

$$[I_{3\phi}] = \begin{bmatrix} i_1(1) & i_1(2) & \cdots & i_1(K) \\ i_2(1) & i_2(2) & \cdots & i_2(K) \\ i_3(1) & i_3(2) & \cdots & i_3(K) \end{bmatrix} \qquad (7)$$

A_{DQ} is the spatial arrangement matrix of the sensor for the three-phase system and $I_{3\phi}$ is the matrix of current time samples $i_n(k)$ from each conductor n, and K is the total number of measured samples. The values in the matrix $I_{3\phi}$ are obtained from the simulation described in the next section.

III. Simulation

In this section, a realistic model of TL is proposed in order to perform several simulations of fault for subsequently validating the fault location method. The simulation was performed using Simulink/Matlab® and the toolbox SimPowerSystems™.

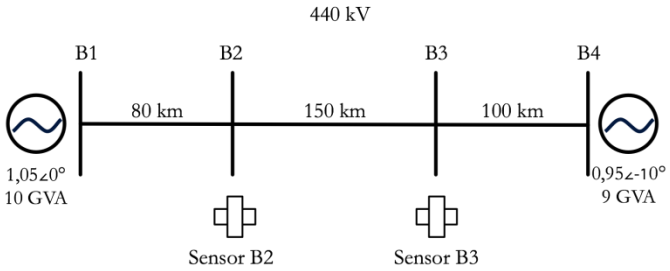

Fig. 2 - Electric power system analyzed

A. Transmission line model

The model proposed for the transmission line is similar to that described in [19], which is 150 km long and 440 kV; see Fig. 2. Note that the performance and behavior of a TL depends almost exclusively on its dimensions and physical parameters. Thus, it is important to determine the electrical parameters of the TL to be used in the simulation.The TL used as a sensitive case for this work is a typical line of *Companhia Energética de São Paulo* (CESP) between the cities of *Bauru* and *Jupiá* in Brazil. Fig. 2 shows the EPS analyzed, which uses two generators, the first being 10 GVA, 440 kV and 0° phase angle, and the second, 9 GVA, 440 kV and -10° phase angle. The system is composed of 3 segments, B1-B2, B2-B3 and B3-B4, of length 80 km, 150 km and 100 km respectively. For this work, all the faults simulations are performed within the central segment B2-B3, and the measurements of the magnetic field are made in the vicinity of the Busbars B2 and B3.

Based on these physical parameters, the electrical parameters of the system are computed. They are the resistances, capacitances and inductance of the positive and zero sequences, as shown in Table 1.

TABLE 1
RESISTANCES, CAPACITANCES AND INDUCTANCE OF THE LT.

Sequences	Resistances (Ω/Km)	Capacitances $(\mu F/Km)$	Inductance (mH/Km)
Zero	0.023	12.259	0.937
Positive	0.299	7.103	3.299

These parameters are important not only for simulation, but also to calculate the speed of wave propagation in the TL. The following equation shows the wave propagation velocity, denoted u_m, in the modeled TL:

$$u_m = \frac{1}{\sqrt{L_0 C_0}} = 295.045\ km/s \qquad (8)$$

Where L_0 and C_0 are the inductance and the capacitance zero sequence.

As shown in Fig. 3, the magnetic field sensors are positioned in the vicinity of the TL. We calculated the A_{DQ} matrix and then the horizontal H_x and vertical H_y components of the magnetic field through (5). The sensors were arranged under Busbar B2 and Busbar B3, as shown in Fig. 2.

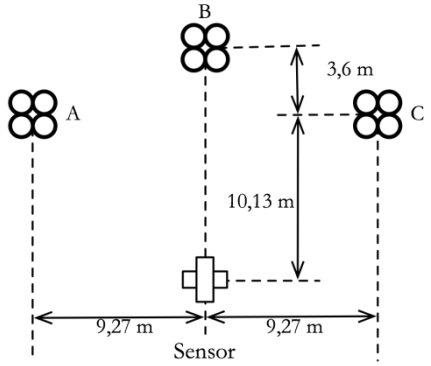

Fig. 3 - Arrangements of the sensors near the TL

For fault monitoring, we consider the squared magnitude of the magnetic field, due to its sinusoidal characteristics:

$$|H(k)|^2 = H_x(k)^2 + H_y(k)^2 \qquad (9)$$

B. Simulation database

To obtain the database, some aspects of the simulation have to be highlighted. Among them, we have the simulation sampling frequency f_s. This frequency should be high enough to properly represent the transitory phenomena and in addition, to provide the desired fault location accuracy. Taking these two factors into consideration, the sampling frequency was chosen at 1.5 MHz. With this frequency, it is possible to observe frequencies up to 750 kHz according to the Nyquist theorem, and to obtain an accuracy of 98 m, as shown in [17]. Each simulation lasted 0.1 s, i.e., 6 periods of 60 Hz.

The system must simulate several faults according to different values of the main parameters that affect the amplitude and the transition of the faults. In this study four parameters have been taken into account: the type, the angle, the resistance (Rf) and the location of the fault.

The fault distance, which is the distance between the swing Busbar (B2) to the point where there was a fault, was simulated from 5 km to 145 km with 20 km intervals. For each distance, 1000 cases were simulated with random values of the other parameters, which represent a total of 8000 cases. Table 2 shows a summary of the parameters, their ranges and the points taken into account in the simulation.

TABLE 2
SUMMARY OF THE SIMULATION PARAMETERS

Parameters	Description	Range	Choice
Types of faults	3 - Phase to ground 3 - Phase to phase 3 - Two phases to ground 1 - Three-phase	1-10 cases	rand
Angle of fault	The inception angle	0°-180°	rand
Fault resistance	The resistance which caused the fault	1-100 Ω	rand
Fault distance	Where occur the fault	$5km$-$145km$	$\triangle$ $20km$

IV. METHODOLOGY

The proposed fault location methodology is based on the analysis of the magnetic signature $x(k) = |H(k)|^2$ captured by the two sensors, B2 and B3 (see Fig. 2 and Fig. 3 and (9)). For each signal, an Auto-Regressive (AR) model is first identified. Based on this model, the magnetic signature is predicted one step ahead and the prediction error is computed. Once this error overcomes a threshold, a disturbance is assumed to have occurred in the system. According to the times of occurrence detected by each of the two sensors, the fault location can be evaluated according to the traveling wave theory.

This methodology thus needs three steps, model identification, fault detection and fault location, which are described in greater detail in the three subsections as follows.

A. Model identification

An m-th order AR model assumes that each sample $x(k)$ of a signal is a linear combination of the m previous samples $x(k-n)$; thus

$$x(k) = \sum_{n=1}^{m} a_n x(k-n). \qquad (10)$$

Where a_n is the n-th coefficient of the AR model. The AR models are particularly suitable to the signals presenting strong spectral content at a limited number of frequencies as is the case for sinusoidal and harmonic signals.

To identify the value of the AR coefficients that best describe the squared magnetic field $|H(k)|^2$ measured by the sensors, a mean squared algorithm [20] is applied to the first two periods of the signals (16.67ms). Considering the signals from the simulation presented in the previous section, a 6th-order model was found to be adapted.

B. Fault Detection

Once the AR model has been identified, the magnetic signature at time k can be predicted as a function of the true signature measured at the previous times according to

$$\hat{x}(k) = \sum_{n=1}^{6} a_n |H(k-n)|^2. \qquad (11)$$

Where $\hat{x}$ denotes the estimate of $|H|^2$. At every sample time k, the prediction error $\varepsilon(k)$ is then evaluated according to

$$\varepsilon(k) = \hat{x}(k) - |H(k)|^2 \qquad (12)$$

An abrupt variation in the prediction error indicates that the magnetic signatures measured at the sensors are no longer consistent with the previously identified model. It can therefore be concluded that a disturbance has occurred in the TL. In the methodology proposed, the detection of a fault is achieved by monitoring the prediction error (12) and comparing it with a threshold ε_{th}. If $\varepsilon(k) > \varepsilon_{th}$, a fault is detected.

The detection threshold ε_{th} is obviously a critical parameter of the method: a high threshold could lead to misdetections, while a too small threshold would detect numerous wrong

faults. In this study, the threshold is chosen to be 110% of the maximum prediction error observed during the two periods which follow the model identification step (between 16.67ms and 33.33ms); hence, we have

$$\varepsilon_{th} = 1.1 * \max_{16<t<33} \varepsilon(k). \quad (13)$$

Fig. 4 illustrates these two stages divided by the dashed red line. The blue signals represent the magnetic signature (left side & top) and the prediction error (left side & down) during the AR model identification stage, and the black signals (right side) correspond to the threshold determination stage.

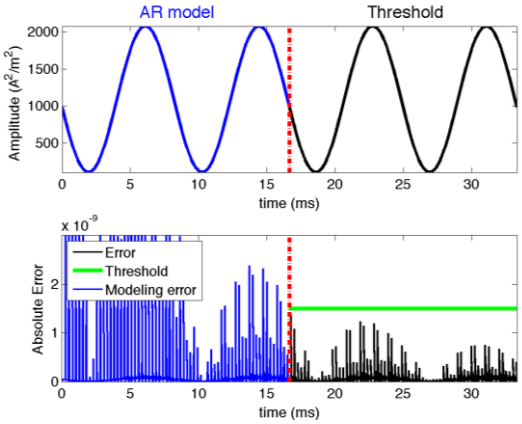

Fig. 4 – Two stages of the method: AR model identification (left side or blue signals) and detection threshold determination (right side or black signals). Top: simulated magnetic signature. Down: prediction error.

C. Fault Location

Based on the difference between the times of occurrence of the fault in the two TL terminals, the travelling wave theory [22][23] allows determining the location of the fault along the TL.

Denoting d_1 and d_2, the distances between the location of the disturbance and the two sensors, l is the length of the TL, u_m the propagation speed of the electrical wave along the TL and t_1 and t_2 the times of fault detection for the two sensors, we have the following equations:

$$l = d_1 + d_2 \quad (14)$$

$$d_1 = u_m t_1 \quad and \quad d_2 = u_m t_2 \quad (15)$$

Putting those equations together, the distance d_1 between the fault and the first sensor can be obtained as

$$d_1 = \frac{l - u_m(t_2 - t_1)}{2} \quad (16)$$

The latter equation is used to estimate the fault location.

V. Results

In this section, we evaluate the performance of the methodology proposed based on AR modeling to locate potential faults in a TL. We also present some results to illustrate the simulations.

A. Simulation results

In order to illustrate the simulated data, Fig. 5 and Fig. 6 show the data from a simulation of a three-phase fault, located 100 km away from Busbar B2, with Rf=50 Ω and 0° of incidence angle. The figures show the currents in the three phases and the squared magnitude of the magnetic field.

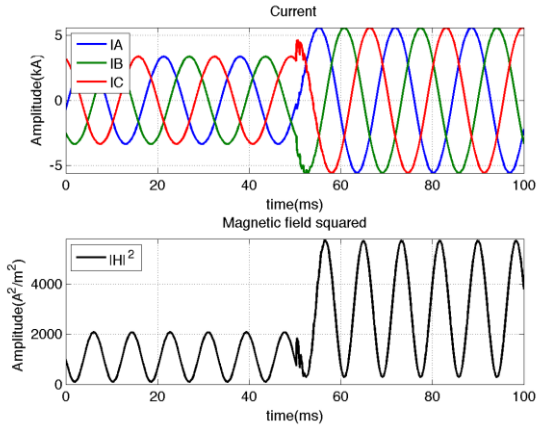

Fig. 5 - Signals of three-phase current and magnetic field squared of a three-phase fault measured at Busbar B2

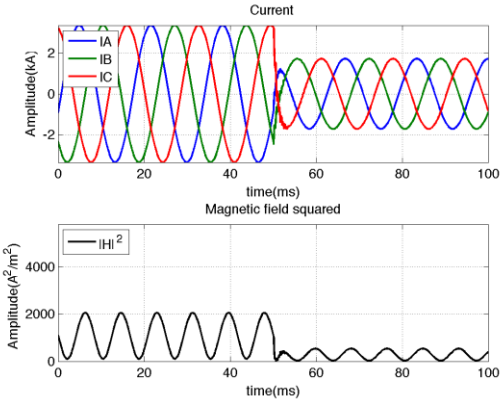

Fig. 6 - Signals of three-phase current and magnetic field squared of a three-phase fault measured at Busbar B3

Note that, the fault transient can be verified in both signals: the current signals and the squared magnetic field.

B. Fault detection and location

In order to exemplify the AR detection and location algorithms, we simulate a fault at 100 km of the TL and estimate the AR model of the squared magnetic field in the first 16.67 ms. The AR coefficients obtained from Busbar B2 in this example give the following prediction equation:

$$\hat{x}(k) = 4.0\,H(k-1)^2 - 6.8\,H(k-2)^2 - 6.5\,H(k-3)^2 - 4.0\,H(k-4)^2 - 1.5\,H(k-5)^2 + 0.28\,H(k-6)^2 \quad (17)$$

The value of the detection threshold calculated in this example for Busbar B2 was $1.5x10^{-9}$.

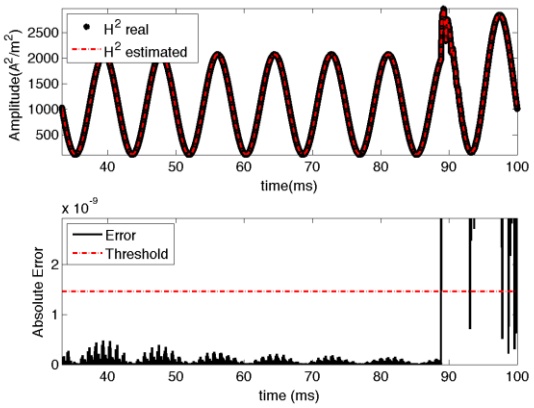

Fig. 7 - Estimation error on the terminal B2- AR model

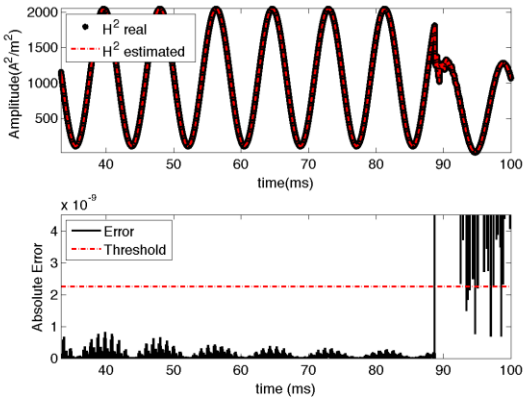

Fig. 8 - Estimation error on the terminal B3- AR model

Fig. 7 and Fig. 8 show the estimated signal of the magnetic field and the absolute error between the estimated value and the actual value, at terminals B2 and B3, respectively. The error signal crosses the threshold at time $t_1 = 88.8580$ ms for the terminal B2 and at time $t_2 = 88.6887\ ms$ for the terminal B3. The difference between the detection times is then $t_2 - t_1 = -0.1693\ ms$.

After estimating the occurrence time of the fault for each line terminal, the time data are processed using the traveling wave technique as described in Section IV.C. From the value of $t_2 - t_1$, the distance at which the fault occurred is calculated. For this example, we obtained an estimated distance of $\hat{d}_1 = 99.98\ km$ and an error of 24 m.

C. Global results

The 150 km TL system was simulated to evaluate the global performance of the methodology. Different cases were simulated, varying the parameters that can significantly affect the system behavior (see Section III).

Table 3 shows the global results applying the methodology for the 8000 cases simulated. The error has been calculated by $(\hat{d}_1 - d_1)$ for all cases; where, $\hat{d}_1$is the estimate distance.

TABLE 3
RESULTS OF LOCATION ALGORITHMS

Mean error	STD	Sampling uncertainty
$0\,m$	$0.028\,m$	$\pm 49.174\,m$

Table 3 allows observing the suitability of the model in many situations, which is highlighted by the results of the mean errors. The sampling uncertainty is related to the choice of f_s (sampling frequency), thus, regardless of the methodology adopted, the traveling wave-based method can not get a better accuracy than that.

VI. CONCLUSION

An analysis of the feasibility of locating faults in EPS based on non-invasive measurements was presented. The methodology proposed relies on the AR modeling of the magnetic field generated by the TL.

The results show the potential of the methodology. The average error obtained by applying the AR modeling estimator was considered satisfactory. The maximum error obtained was 39 m. The algorithm showed good performance, independently of the parameters that affect the waveform of the fault.

In addition, the method is not dependent on fault resistance, as the current distance relays; and it does not need previous simulations to be implemented, as the methods involving machine learning.

The use of a non-invasive approach to solve problems related to fault location can be a promising alternative, regarding its capacity to monitor the system information based on the magnetic field, not requiring accessories connected to TLs. The method is limited by the signal sampling frequency and by the techniques required by the hardware; physical implementation will be considered in future studies.

Moreover, the angle between the signal components in horizontal and vertical direction and the magnetic field are likely to considerably improve to the fault detection avoiding false alarms, in addition to a great potential for fault classification.

We can propose new methodologies exploring the noninvasive feature. The literature shows several techniques with invasive proposals that we could extensively explore. The standard analysis in the frequency domain associated with computational intelligence techniques can yield good results as well as the methods already analyzed for invasive approaches.

As the noninvasive analysis is a new approach in the literature, the possibilities of new fault location techniques are manifold and may exploit not only location but also classification, harmonic monitoring, protection, among others.

VII. ACKNOWLEDGMENT

The Authors would like to acknowledge the effort of the Maxwell Associate International Laboratory (LIA CNPq/CNRS) and specifically of its french coordinator L. Krähenbühl, as well as the Brazilian Navy for their supports in the development of this work.

VIII. REFERENCES

[1] COURY, D. V. Um estimador ótimo aplicado à proteção dos sistemas elétricos de potência. 1987. Tese de Doutorado. Dissertação (Mestrado) - Escola de Engenharia de São Carlos, Universidade de São Paulo.

[2] LAIN, B.; SALAMA, M. M. A. An overview of the digital fault location algorithms for the power transmission line protection based on the steadystate phasor approaches. 1996.
[3] CHENG, Y. et al. One-terminal impedance fault location algorithm for single phase to earth fault of transmission line. In: Power and Energy Engineering Conference (APPEEC), 2010 Asia-Pacic. [S.l.: s.n.], 2010. p. 1-6.
[4] LIMA, D. et al. Electrical power systems fault location with one-terminal data using estimated remote source impedance. In: Power and Energy Society General Meeting (PES), 2013 IEEE. [S.l.: s.n.], 2013. p. 1-5. ISSN 1944-9925.
[5] KEZUNOVIC, Mladen. Smart fault location for smart grids. Smart Grid, IEEE Transactions on, v. 2, n. 1, p. 11-22, 2011.
[6] SAHA, M. M.; IZYKOWSKI, J. J.; ROSOLOWSKI, E. Fault location on power networks. [S.l.]: Springer Science & Business Media, 2009.
[7] NIAZY, I.; SADEH, J. Wavelet-based one-terminal fault location algorithm for aged cables without using cable parameters applying fault clearing voltage transients. In: Power System Technology (POWERCON), 2010 International Conference on. [S.l.: s.n.], 2010. p. 1-6.
[8] MEGAHED, A. et al. Wavelet based fault location technique for two and three terminal lines. In: Power and Energy Society General Meeting, 2012 IEEE. [S.l.: s.n.], 2012. p. 1{7. ISSN 1944-9925.
[9] LI, Z. Hilbert-huang transform based application in power system fault detection. In: Intelligent Systems and Applications, 2009. ISA 2009. International Workshop on. [S.l.:s.n.], 2009. p. 1-4.
[10] CHANDA, N.; FU, Y. ANN-based fault classification and location in mvdc shipboard power systems. In: North American Power Symposium (NAPS), 2011. [S.l.: s.n.], 2011. p. 1-7.
[11] GIOVANINI, R.; COURY, D. Classificação rápida de faltas em sistemas elétricos utilizando redes neurais artificiais. Proceedings of the IV Brazilian Conference on Neural Networks - IV Congresso Brasileiro de Redes Neurais pp. 281-286, July 20-22, 1999.
[12] JORGE D.C.AND COURY, D. Artificial neural network approach to distance protection of transmission lines. IEEE Transactions on Power Delivery, v. 13, n. 1, p. 102-108, Janeiro 1998.
[13] PURUSHOTHAMA, G. K.; NARENDRANATH, A. U.; THUKARAM D.AND PARTHASARATHY, K. ANN applications in fault locators. ELSEVIER Electrical Power and Energy Systems, v. 23, 2008.
[14] MORETO, M. localização de faltas de alta impedância em sistemas de distribuição de energia: uma metodologia baseada em redes neurais artificiais. Dissertação Apresentada a UFRS., 2005.
[15] NETO, J. A. O.; CASTRO, M. A. A.; VIEIRA, G. M., FELIX, L. B. Classificação e localização de faltas em um sistema de distribuição industrial contendo harmônicos. The 8th Latin-American Congress on Electricity Generation and Transmission - Clagtee 2009, Clagtee, v. 8, n. B-672, 2009.
[16] SARTORI, C. A. F.; SEVEGNANI, F. X. Fault classification and detection by wavelet-based magnetic signature recognition. Magnetics, IEEE Transactions on, IEEE, v. 46, n. 8, p. 2880-2883, 2010.
[17] FERREIRA, K. J.; EMANUEL, A. E. A noninvasive technique for fault detection and location. Power Delivery, IEEE Transactions on, IEEE, v.25, n.4, p. 3024-3034, 2010.
[18] EMANUEL, A. E. et al. A non-contact technique for determining harmonic currents present in individual conductors of overhead lines. Power Apparatus and Systems, IEEE Transactions on, n. 3, p. 596-603, 1983.
[19] OLESKOVICZ, M.; COURY, D. V.; AGGARWAL, R. K. Redes Neurais Artificiais aplicadas à classificação rápida de faltas em sistemas.
[20] MARPLE JR, S. Lawrence. Digital spectral analysis with applications. Englewood Cliffs, NJ, Prentice-Hall, Inc., 1987, 512 p., v. 1, 1987.
[21] NISHIYAMA, Kiyoshi. A nonlinear filter for estimating a sinusoidal signal and its parameters in white noise: on the case of a single sinusoid. Signal Processing, IEEE Transactions on, v. 45, n. 4, p. 970-981, 1997.
[22] MAGNAGO, F. H.; ABUR, A. Fault location using wavelets. Transactions on Power Delivery, IEEE, v.13, n. 4, p. 1475-1480, 1998.
[23] MAGNAGO, F. H.; ABUR, A. IEEE guide for determining fault location on ac transmission and distribution lines. EEE Standard, IEEE, n. C37.114, p. 1475-1480, 2004.
[24] AL-MOHAMMED, A. H.; ABIDO, M. A. An adaptive fault location algorithm for power system networks based on synchrophasor measurements. Electric Power Systems Research, v. 108, p. 153-163, 2014.

IX. BIOGRAPHIES

Jésus Anício de Oliveira Neto - degree in Electrical Engineering from the Federal University of Viçosa (2011). He is currently a lieutenant engineer with the Brazilian Navy at *Centro Tecnológico da Marinha* in *Sao Paulo* and a Master's student at the Escola Politécnica of the University of São Paulo (Poli / USP). Experienced in Electrical Engineering, mainly in the following subjects: Signal Processing, Biomedical Engineering, Power Distribution Systems.

Carlos Antonio França Sartori - (SM'91) received his B.Sc., M.Sc., and Ph.D. degrees from Escola Politécnica of the University of São Paulo (EPUSP), in 1983, 1994, and 1999, all of them in Electrical Engineering. In 1984, he joined the National Commission on Nuclear Energy CNEN/IPEN-SP, where he is the technical lead responsible of the Electromagnetic Compatibility (EMC) Group. He is an Invited Professor at the Graduate Programs of EPUSP (1999) and at the Nuclear and Energy Research Institute IPEN-CNEN/SP (2006), and an Associate Professor at the Catholic University of São Paulo, where he was the Vice-head of the Department of Electrical Engineering (1997-1998), and the Vice-Dean (2001-2004). He is a member of the IEEE EMC Society (SM'91), the IEEE South Brazil EMC Chapter Chair, and an EMC Board of Directors Member. He is also a member of the International Compumag Society, and of the Brazilian Society on Electromagnetics, where he was the Vice-president (1998 to 2002). His current research interests include applied electromagnetics and EMC problem modeling such as lightning, transmission line coupling, new measurement techniques, evaluation of equivalent sources and evaluation of electromagnetic environment, risk analysis and biologic effects.

Eric Blanco - From 1998 to 2003, he was engaged in research on robust estimation problems in the Laboratory of Process Control and Chemical Engineering (LAGEP). Since 2003, he has been an Assistant Professor of automatic and signal processing in the Ecole Centrale de Lyon, Ecully, France. He is also with the Centre National de la Recherche Scientifique (CNRS), Unités Mixtes de Recherche (UMR) 5005, Laboratoire AMPERE, Villeurbanne, France, where he is engaged in diagnosis, estimation, and prediction of complex system.

Julien Huillery - Received his M.S. degree in Electrical Engineering from the École Supérieure d'Électricité (France) and the University of Wollongong (Australia) in 2002, the master of research degree in Signal Processing from the University of Rennes (France) in 2004 and his Ph.D. degree in Signal Processing from the university of Grenoble (France) in 2008. After a one-year post-doctoral research position in underwater acoustic communications at the University of Algarve (Portugal), he served as an assistant professor in Signal Processing and Control at the University of Grenoble. Since 2010, he has held an associate professor position at the Electrical Engineering department of the École Centrale de Lyon, France. His research interests concern non-stationary signals and systems analysis, statistical signal processing and information theory. His current projects include signal design for wireless energy transmission, identification and filtering of time-varying systems and stochastic optimization in biological systems.